Reactivity of Polycyclic Aromatic Hydrocarbon Soot Precursors: Implications of Localised π-Radicals on Rim-based Pentagonal Rings

Jacob W. Martin,[†,‡] Dingyu Hou,[¶,§] Angiras Menon,[†,‡] Laura Pascazio,[†] Jethro Akroyd,[†] Xiaoqing You,[¶,§] and Markus Kraft[*,†,‖,‡,⊥]

†*Department of Chemical Engineering and Biotechnology, University of Cambridge, Cambridge CB3 0AS, UK*

‡*Cambridge Centre for Advanced Research and Education in Singapore (CARES), Singapore 138602*

¶*Center for Combustion Energy, Tsinghua University, Beijing, 100084, China*

§*Key Laboratory for Thermal Science and Power Engineering of Ministry of Education, Tsinghua University, Beijing, 100084, China*

‖*School of Chemical and Biomedical Engineering, Nanyang Technological University, Singapore 637459*

⊥*Current address: West Site, Philippa Fawcett Drive, Cambridge CB3 0AS, UK*

E-mail: mk306@cam.ac.uk

Phone: +44 (0)1223 762784

ABSTRACT

This paper presents a systematic study of the reactivity of polycyclic aromatic hydrocarbons (PAH), identifying crosslinks that permit the combination of physical π-stacking interactions and covalent bonding. Hybrid density functional theory was used to identify the location of reactive sites on PAHs using the average local ionisation potential. The bond energies formed between these various reactive sites were then computed. σ-radicals were found to be the most reactive, forming bonds with other radicals and some reactive closed shell edge types. Partially saturated rim-based pentagonal rings were found to form localised π-radicals with high reactivity. This site, in addition to resonantly stabilised π-radicals, was found to be capable of bonding and stacking, which is explored for a variety of larger species. Localised π-radicals on rim-based pentagonal rings, in particular, were found to form strongly bound stacked complexes indicating a potentially important role in soot formation.

INTRODUCTION

Soot emitted from human activities leads to respiratory disease, contributes to warming the atmosphere and increasing ice loss.[1–3] Significant research efforts to understand the mechanisms responsible for the formation of soot are ongoing. The critical stage of soot formation (and the least well understood) is the inception process, in which gas phase aromatics form condensed clusters, resulting in carbonaceous nanoparticles.[4]

Reactive aromatic species have long been thought to contribute to soot inception.[5,6] These species can be grouped into either open shell radical or closed shell aromatic species. The former are significantly more reactive but are present in lower concentrations, and the latter less reactive and are present in higher concentrations. Therefore, reactions between radical species and closed shell species are often the focus of soot mechanisms. Beginning with the radicals, the most well studied reactive species, σ-radicals, are generated by hydrogen being abstracted from the rim of aromatics by collision with gas phase radicals.[7]

This reactive site combined with acetylene addition allows for the extension of the aromatic network through the well known hydrogen abstraction acetylene addition (HACA) growth mechanism.[8,9] Radicals can also arise in the π-bonding network if there is an odd number of π-electrons. These π-radicals can be stabilised due to delocalisation, providing long-lived resonantly stabilised radicals (RSR), although these have reduced reactivity. They are critical for the formation of the first aromatic ring[10] and have long been suggested to be present in aromatic species, indicated by the odd-numbered carbon species measured using flame mass spectrometry.[11] High-resolution atomic force microscopy (HR-AFM) and photoionisation mass spectrometry (PIMS) have also recently confirmed the presence of RSR.[12,13] It was suggested that these react with polycyclic aromatic hydrocarbons (PAH) σ-radicals leading to a chemical polymerisation that did not require subsequent hydrogen abstraction.[13] However, Keller et al.[11] found that for PAH with molecular mass greater than 400 Da odd-numbered carbon fragments in mass spectrometry were of similar concentration to even-numbered carbon fragments (more likely to be closed shell), suggesting that the growth mechanism does not favour reactions with RSR. Evidence for another π-radical has recently been found that arises from a partially protonated rim-based pentagonal ring.[12] This site has been found to have important implications for PAH edge reconstructions and growth[14,15] but it's reactivity with other PAH is unknown.

The aromatic σ- and π-radicals have also been suggested to react with closed shell species that possess significantly electrophilic sites such as double or triple bonds. This is well illustrated by the reaction between the aromatic σ-radical with the acetylene triple bond, which is critical for the HACA mechanism, but is not rapid enough to explain on its own soot particle formation.[9] Benzene and high symmetry aromatic species are strongly aromatically stabilised leading to aromatic bonds with low reactivity compared with double bonded carbon. However, in many low symmetry polycyclic aromatic hydrocarbons, some rings possess a reduced aromaticity. Well known examples are the 9,10-free edge of phenanthrene and pyrene, which is more vulnerable to electrophilic or free radical attack.[16] Rim-based pentag-

onal rings have also been observed and shown to be thermally stable.[17,18] Five-membered rings are not aromatically stabilised and thus provide a free edge with double-bond character and significant reactivity. These low aromaticity free edges have been suggested to react with carbon σ-radicals, forming nanoparticles in the flame through the aromatic aliphatically linked hydrocarbon (AALH) mechanism.[19,20] Evidence for this growth mode has been shown by mass spectrometry of benzene-oxygen flames where high radical concentrations allow for significant carbon σ-radical concentrations.[20] Partial integration of the pentagonal ring within the hexagonal network has been directly imaged[21] and provides edges with greater reactivity, with HACA growth on the five-membered bay site found to proceed rapidly.[22] Fully integrated pentagonal rings curve the aromatic network and have been experimentally observed[23,24] and theoretically predicted.[15] This curvature leads to an electric polarisation of the π-electrons[25] and reduced aromaticity[26] due to reduced π-overlap on pyramidalised carbon atoms. This has been shown to modify the edge oxidation reactivity[27–29] and speed up HACA growth on an armchair edge of hexagonal rings.[22] This curvature integrates a permanent dipole moment into the molecules, suggesting strong dipole-ion interactions are possible, which have been proposed as a possible explanation of the electrical aspects of soot formation.[24] The presence of these reactive aromatics leads to a number of questions: how does the reactivity of different sites compare? How thermally stable are the crosslinks formed between these sites?

The proposed chemical inception mechanisms involving reactive aromatics are not fast enough to explain the experimental observations.[4] Physical condensation, however, could be rapid enough to explain soot formation if sufficient intermolecular interactions existed between the fragments .[9] Direct evidence for physical dimerisation has been found using mass spectrometry of species sampled from the flame, revealing a series of peaked distributions separated by approximately 500 Da (without any change in the C/H ratio, which would imply a chemical reaction).[30,31] Laser induced fluorescence (LIF) experiments have provided evidence for π-stacked aromatics that are able to form an excited eximer state.[32]

Time resolved LIF has shown this signal to be long lived, providing further evidence for the stacked eximer hypothesis.[33,34] However, we have shown that van der Waals or physical dispersion interactions are not sufficient to allow the 500 Da aromatic species (as commonly found in flames) to cluster at temperatures in the flame where soot forms, 1500–2000 K.[35] Previous authors have suggested a combination of covalent bonding and physical interactions to explain the rapid condensation.[6,36,37] A recent electron spin resonance study found a significant reduction in concentration and change in the radical character when soot growth begins indicating a significant number of radical termination reactions occurring at soot inception.[38] In this study authors suggested a combination of physical stacking interactions and covalent bonding between π-radicals such as pancake bonds (multicentre π-bonds)[38] with other suggesting biradical [4] to provide the significant intermolecular interactions required to hold PAH within clusters at flame temperatures. This poses a further question: can a combination of physical interaction and covalent bonding explain the rapid growth of soot?

Computational techniques have reached a level of accuracy and speed that such questions can now be systematically answered. The reactivity of different sites on aromatic molecules can now be predicted directly from the ground state electronic structure using chemical reactivity theory.[39] Thermal stability of aromatic crosslinks requires highly accurate energies that are now possible from hybrid meta-GGA density functional theory such as M06-2X,[40] providing bond energies to within a few kcal/mol and transitions states to within 3–7 kcal/mol.[7,29,41] Finally, physical interactions in stacked aromatic configurations can now be included into density functional methods with empirical dispersion corrections (DFT-D), however, these corrections have been found to systematically overbind PAH.[42] We have recently performed highly accurate benchmark calculations of PAH dimers that allows this systematic overbinding to be quantified and corrected for,[35] allowing physical interactions and chemical bonding to be directly compared.

In this paper, we aim to explore the above mentioned questions using the computational

techniques discussed above. The question of *how the reactivity of different sites compares* is approached by calculating the average local ionisation potential computed on a range of aromatic molecules. *How thermally stable the crosslinks formed between these sites* is systematically determined from calculating the bond energies between the set of reactive sites revealed by the previous analysis. Finally the question of *whether the combination of physical interaction and covalent bonding can explain the rapid growth of soot* is explored for stacked complexes of localised and resonantly stabilised π-radical using dispersion corrected density functional methods, providing important insights into how reactive PAH contribute to soot formation.

METHODS

For determining the minima and transition state geometries we employed a range of electronic structure methods computed in the Gaussian 09 package.[43] For all geometries, frequency calculations were performed to confirm the minima or transition state and also to compute the zero-point energy correction to the electronic structures. We have previously benchmarked a range of hybrid density functional theory methods against experimental and wavefunction methods.[7] We found geometry optimisations at the B3LYP/6-311G(d,p) level of theory and single point calculations at the M06-2X/cc-pVTZ level of theory provide energetics within chemical accuracy for hydrogen abstractions (<1 kcal/mol).[7] Benchmark calculations on hydrocarbon bond energies are found to have a mean unsigned error of 1.78 kcal/mol for this functional.[41]

For the aromatic complexes we have previously found that dispersion corrected B97 hybrid density functional theory performs well for geometries and electrostatics describing the dipole moment of curved arenes.[44,45] A number of geometry optimisations were performed for each edge couple to determine the lowest energy isomer. The B97D/cc-pVTZ level of theory was used in order to ensure minimal basis set superposition errors (<2 kcal/mol) as

the bonded and stacked geometries were unable to be corrected for this error (counterpoise corrected). The bond dissociation energies were calculated from a homolytic bond cleavage using single point energies calculated using the dispersion corrected hybrid density functional M06-2X-D3/cc-pVTZ, which uses the same dispersion correction that was added to the B97D functional but provides significantly better bond energies, as will be detailed in the next section. We compared the van der Waals complexes with our reference SAPT(DFT) calculations[35,46] and found the DFT calculations to overestimate the binding energy by -6 ± 1 kcal/mol, which will be further discussed in the results section.

The average local ionisation potential is used to locate and compare reactive sites on aromatic species to electrophilic attack by, for example, carbon radicals[47] and is computed as,

$$\bar{I}(\mathbf{r}) = \sum_{i}^{N_{occ}} \frac{\rho_i(\mathbf{r})|\epsilon_i|}{\rho_{tot}(\mathbf{r})}, \tag{1}$$

where ρ_i is the electron density of the i-th molecular orbital at the point $\mathbf{r}$, ϵ_i is the orbital energy and $\rho_{tot}(\mathbf{r})$ is the total electron density at the point $\mathbf{r}$ where the sum is over the N_{occ} occupied molecule orbitals. $\bar{I}(\mathbf{r})$ is then a local measure of the energy required to ionise an electron from a certain point in space and therefore a lower value indicates a higher reactivity to electrophiles such as radicals. The Fukui function $f^-(\mathbf{r})$ has also been used to compute the reactivity of sites towards hydrocarbon radicals in the context of soot.[48] $f^-(\mathbf{r})$ requires that the electron density of the ionised molecule be computed and the difference taken with the molecule in its standard state. This is often approximated with the highest occupied molecular orbital (HOMO), but this is not possible for larger aromatics with many low lying occupied molecular orbitals that could also contribute, e.g. HOMO–1, HOMO–2 etc. Therefore, two calculations would be required to compute $f^-(\mathbf{r})$. The average local ionisation potential and the Fukui functions are formally related in the local density approximation as $\bar{I}(\mathbf{r}) = \sum_i |\epsilon_i| f_i^-(\mathbf{r})$, where the index is over the i-th occupied molecular orbitals, indicating they will both provide the most electrophilic site.[49] The advantage of using $\bar{I}(\mathbf{r})$ is that only

a single electronic structure is required as it considers ionisation from all of the occupied MO while also providing a convenient comparison across our molecular series. Multiwfn 3.3.9 was used to compute the average local ionisation potential on the isosurface 0.002 atomic units (a.u.) of the electron density (near the van der Waals surface) computed from the electronic structure calculations.[50] We also prepared spin population isosurfaces for the resonantly stabilised radicals using Multiwfn.

In the context of aromatic species, $\bar{I}(\mathbf{r})$ has been found to accurately predict the sites most reactive to electrophilic attack of hydrogen radicals.[39] To further confirm this we demonstrated that the enthalpy of hydrogenation at edges of closed shell species correlates well with the minima near the edge carbon atom that was protonated, $\min_r[\bar{I}(\mathbf{r})]$ (see Figure S1 in the supplementary information). We can then suggest that $\min_r[\bar{I}(\mathbf{r})]$ is appropriate for comparison between the different radical and closed shell species' reactivity. For ease of reading, the minimum in the average local ionisation of the site $\min_r[\bar{I}(\mathbf{r})]$ will be referred to as $\bar{I}_S$.

RESULTS AND DISCUSSION

Reactivity of aromatic edges

Figure 1 shows the average local ionisation potential calculated on the molecular surface for aromatic species ordered by their $\bar{I}_S$. This serves two main purposes: classification and ordering of the different radicals and closed shell species, as well as an understanding of the location of the potential reactive sites that are capable of crosslinking reactions, which will be explored in the next section.

We will begin with closed shell species as they will introduce the concepts of reactivity and aromaticity using the $\bar{I}_S$ metric. Partially embedded cyclopentaphenathrene-type pentagonal rings **(D)** possess the lowest $\bar{I}_S$ site with values $\bar{I}_S = 7.28 - 7.41$ eV. The $\bar{I}_S$ are concentrated on the aromatic face on the pentagonal's edge, with the pentagonal ring being partially embedded with three bond sharing hexagonal rings. This non-aromatic site has

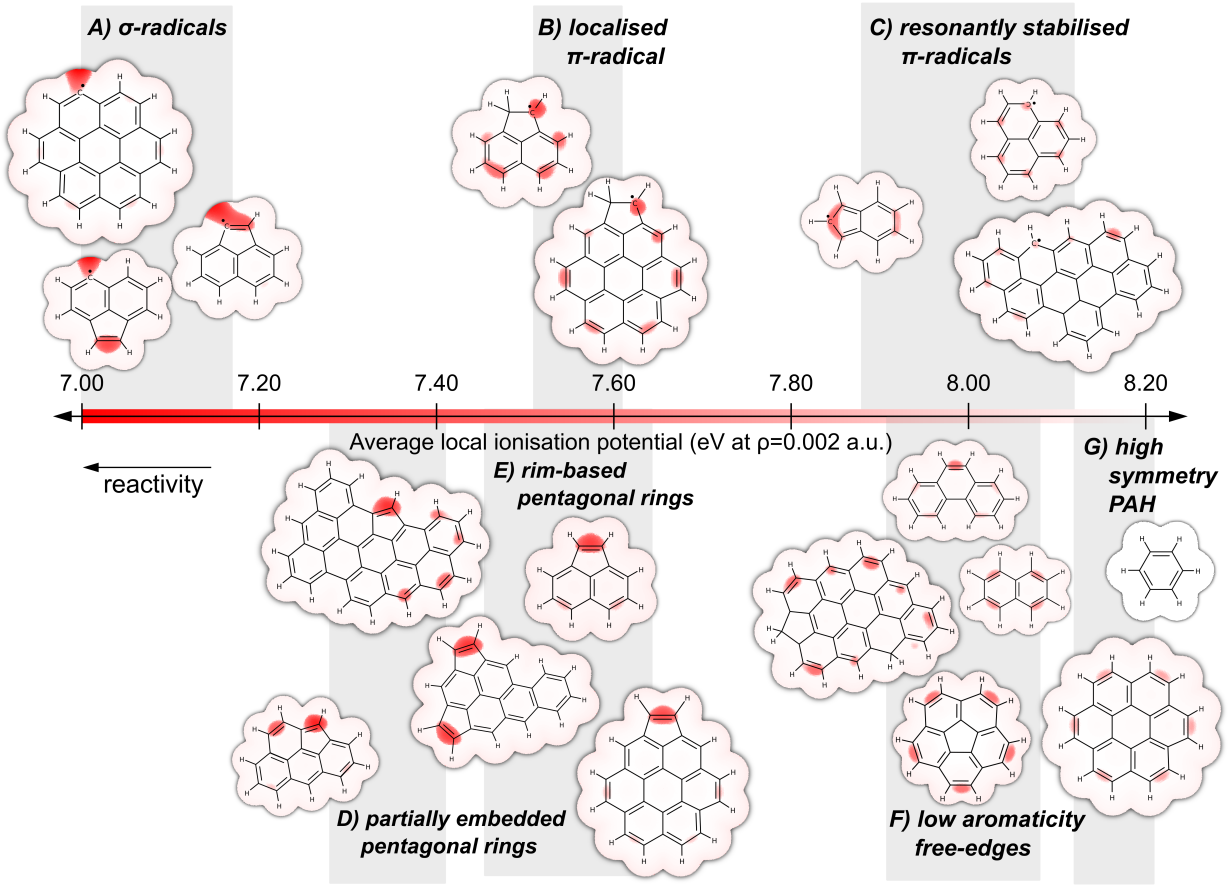

Figure 1: The average localised ionisation potential is plotted on the molecular surface produced from the electron density at the isovalue $\rho = 0.002$ a.u. (B97D/6-311G(d,p)) for a variety of aromatic species. Overlayed on these molecular surfaces are one the Kekulé structures.

been observed in HR-AFM and is an intermediate towards completely curved species.[12] We also explored other partially embedded pentagonal rings that had also been observed, such as fluoranthene or benzo[ghi]pyrene type, but these were found to have $\bar{I}_S$ matching that of low-aromaticity free edges shown in the scheme below.

This indicates that aromaticity is lowest for the cyclopentaphenathrene type edges providing the most reactive configuration of a partially embedded pentagonal ring. This could explain why this site type is most often seen to be methylated, fluorene-like, having two

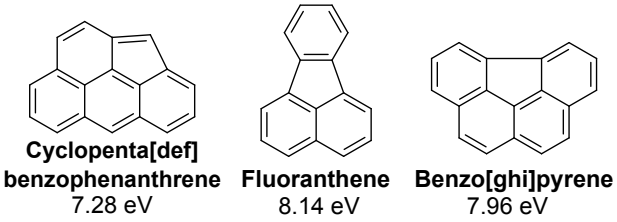

hydrogens bonded to the edge in HR-AFM.[21]

Rim-based pentagonal rings **(E)** possess values of $\bar{I}_S = 7.45 - 7.64$ eV. The minima is concentrated on the edge carbon atoms of the pentagonal ring. In this case only two neighbouring bonds are shared with the hexagonal aromatic rings and due to the antiaromatic pentagonal ring the $\bar{I}$ indicates a free edge with a double-bond character. There is little effect from the system size and many of these sites can be present on a single aromatic. Experimentally this was found to be a common edge type.[21]

Low aromaticity free edges **(F)** possess values of $\bar{I}_S = 7.91 - 8.08$ eV. These arise in hexagonal aromatic networks due to the topology of the network. Clar *et al.* provided a framework for describing these low-aromaticity edges.[16,51] The maximum number of sextets are placed within the network with double bonds placed elsewhere. The symmetrically equivalent arrangements of sextets (denoted by a circle within the ring) and double bonds are then considered to be in resonance in more modern formulations.[52] The edge sites where double bonds are prevalent in the resonance structures are found to be reactive. These Clar descriptions match with the sites with low $\bar{I}_S$ and with the reactivity trends for these species[16] and has been used to describe PAH growth.[53] Some examples are shown in the scheme below.

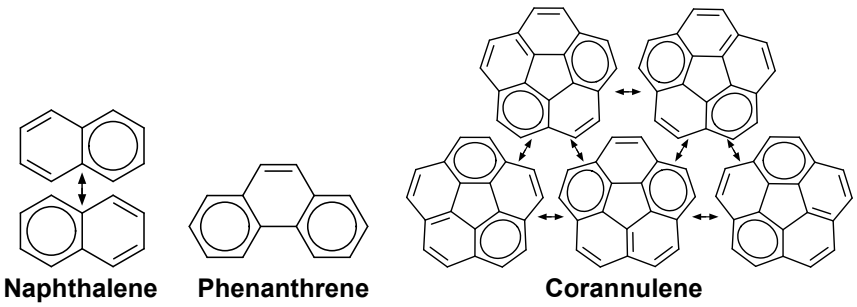

Naphthalene contains a single sextet that is in resonance (otherwise known as a travelling sextet). This allows for the free edges to possess a double-bond character with an increased reactivity. Phenanthrene is an example of a structure with a single Clar structure with two sextets leaving the 9,10-free edge with a significant double bond character and higher reactivity than the rings with the sextets.[16] Corannulene can have two sextets and five resonance structures.[51] This provides low-aromaticity free edges with double-bond character. Corannulene has an added reduction in aromaticity due to the pyramidalisation of the carbon network, as shown by others.[26] This might explain the lower $\bar{I}_S$ compared with phenanthrene or naphthalene found for corannulene. Another cause of low aromaticity edges was methylation of hexagonal aromatic edges site. In the Clar framework this is due to the reduction in the number of sextets that can be placed. Finally, high symmetry PAH **(G)** such as benzene or coronene are found to possess the highest $\bar{I}_S$ value of all of the closed shell edges with values $\bar{I}_S = 8.12 - 8.21$ eV. The symmetry of these species, being close to circular, provides highly pericondensed networks with high aromaticity and no low-aromaticity free edges.

Turning now to the radicals, the site of lowest $\bar{I}_S$ was found to be the σ-radical **(A)** with minimum values from 7.00 – 7.17 eV. The reactive site minima lies on the edge of the aromatic, parallel to the carbon–hydrogen bonds. Little difference was found between the rim-based, pentagon-based σ-radical compared with the hexagonal ring-based one. This reactive site is known to react with acetylene readily and drives the growth of the aromatic network.[9] The next lowest $\bar{I}_S$ is the localised π-radical **(B)** with minimum values from 7.51–7.61 eV. In both cases the minima lies on the rim-based pentagonal carbon atom with a single hydrogen attached. Unlike the σ-radical, the $\bar{I}_S$ is on the face of the aromatic plane. There are also regions of low $\bar{I}$ around the rim, which have similar values to the low aromaticity free edges, indicating this site can modify the other edge sites on the same molecule. This will be further discussed later in the text.

In order to determine the localisation of this radical, two partially saturated pentagonal

rings were added to the seven-ring aromatic coronene (Figure 2a). The triplet with two free electrons (a biradical) was found to be significantly more stable (-24.3 kcal/mol) compared to the singlet. If the radical was able to delocalise across the aromatic network a stable closed shell singlet spin configuration would be more stable. However, as the triplet dominates we can confirm that the radical is indeed localised to the pentagonal ring and that multiple localised π-radicals could be formed on a single aromatic with the low $\bar{I}_S = 7.54\ eV$ preserved as shown in Figure 2a.

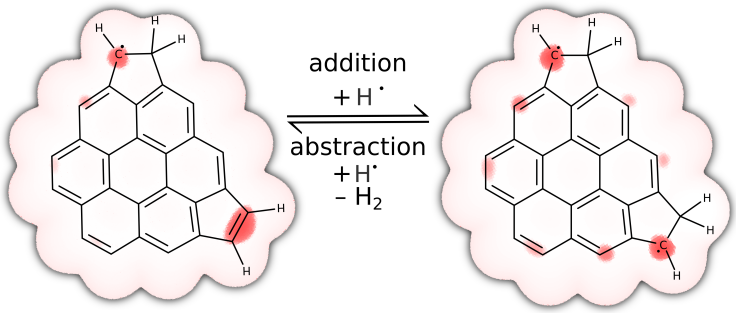

(a) Mechanism for forming two **B)** edge types showing the two independent localised π-radicals.

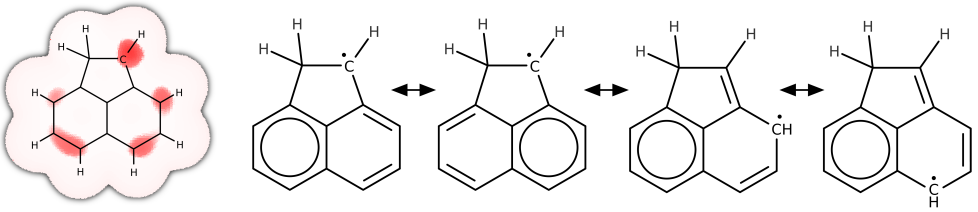

(b) Clar analysis of 1,2dihydroacenaphthylen1yl.

Figure 2: $\bar{I}(\mathbf{r})$ surface plotted as in Figure 1 for the partially hydrogenated edges of type **(B)**.

A Clar analysis provides insight into why the radical is localised (Figure 2b). Considering the average local ionisation potential and spin density of 1,2dihydroacenaphthylen1yl, four major Clar structures can be drawn. The first two resonance structures have a sextet on the hexagonal rings with the radical localised to the pentagonal ring. The third and fourth resonance structures have the radical on the aromatic ring, *i.e.* the β- and δ-position from the

pentagonal site. Similar patterns in the $\bar{I}(\mathbf{r})$ are also found for the larger species in Figure 2a, where the radical site only appears to be delocalised to the β- and δ-position relative to the pentagonal radical site. It can therefore be suggested that the radical is partially localised in order to maintain the high aromaticity of the six-membered ring network.

The radical with the highest $\bar{I}_S$ was found to be the resonantly stabilised π-radical RSR **(C)** with $\bar{I}_S = 7.88 - 8.12$ eV. These arise from an odd number of π-electrons in an aromatic network providing a radical stabilised by delocalisation.[54] The smallest species, indenyl, was found to have the lowest $\bar{I}_S$ value (7.88 eV) concentrated on the surface of the pentagonal ring, while for increasing size the value drops to 8.12 eV and is concentrated on the face of the aromatic on the zig zag edge sites. We will explore later whether this reduction impacts the reactivity of the RSR as they enlarge and the radical becomes more resonantly stabilised.

The reactive edges have been described and grouped. Importantly, the location of reactive sites has been found allowing for potential crosslinks between these reactive sites to be explored on a smaller subset of edges in the following section.

Crosslinking reactions between reactive aromatics

In order to compare the reactivity of a variety of edge types, we have chosen to consider only the first bond formed between a series of small species. There are a number of reasons for this. Firstly, the formation of the first bond will provide insight into the edge site reactivity and provide further evidence for the reactivity ordering predicted from $\bar{I}_S$. Secondly, the first bond is important for the crosslinking reaction as the reaction is not entropically favoured due to a reduction in the number of species, and therefore the energy of the first bond directly corresponds to the likelihood of the complex fragmenting. Thirdly, molecular beam mass spectrometry shows that the clustering process, in low temperature flames, does not involve crosslinking reactions with dehydrogenation but a constant C/H ratio.[30,31] Thirdly, we did not include any aliphatic bridges with methyl or longer aliphatics that have recently been observed in specific inverse diffusion flames.[55] These would modify the C/H ratio and

therefore would represent a different growth mode than what we are focusing on in this study. Furthermore, in premixed flames these aliphatic bridges would be prone to radical-induced fragmentation, just as the fuel is. Therefore, we restricted our search to crosslinks that do not modify the C/H ratio and have been seen in aromatics directly imaged using HR-AFM.[21] Finally we did not consider reactions with the high-symmetry PAH as these were found to form bonds with energies >-30 kcal/mol fragmenting at flame temperatures as discussed below.

Figure 3 shows the matrix of bond energies between the species containing different edge types ordered by their bond energy with the σ-radical. A general trend was found where edge sites with low $\bar{I}_S$ produced more stable bonds compared to those with high $\bar{I}_S$ (as seen in the inset graph). However, steric effects also contribute to these bond energies leading to slightly different orderings compared with $\bar{I}_S$ values. We did find that the site with the lowest $\bar{I}_S$, or its neighbour, was always found to be the most reactive. Bond energies can be compared to the bond enthalpy benchmark values[56] (as the thermal correction is minimal at <1 kcal/mol. The biphenyl C–C bond has a benchmark value of -117.6 kcal/mol;[57] using our methodology provided a value of -119.4 kcal/mol, showing a slight overestimation of the bond energy (+1.5%). Therefore, these values should be viewed within this error to provide a comparative look at the reactivity of the different edge sites. To consider the flame stability of bonded species, a comparison with other species is helpful. The thermal energy necessary for homolytic bond cleavage can be approximated as $6RT$ (3/2RT for the translational and 3/2RT for rotational degrees of freedom for each species), which is 17 kcal/mol at 1500 K and 24 kcal/mol at 2000 K. However, to be persistently stable at flame temperature, larger bond energies have been found to be required. The primary fragmentation pathway for fuels is radical induced fragmentation, such as β-scission, where the β site can have bond energies of -30 – -40 kcal/mol that readily break at flame temperatures.[58] For the physical dimerisation of flat PAH, a full statistical approach revealed that a binding energy of < -40 kcal/mol was required for clustering above 1500 K.[4] Single bonds C–H and C–C in benzene and aliphatics

have bond dissociation energies of −113 and −90 kcal/mol respectively, and require high temperatures for unimolecular decomposition (>2000 K). We therefore consider anything below −40 kcal/mol to be of interest for soot formation and anything above −10 kcal/mol is not considered for forming any thermally stable bond (highlighted red in Figure 3).

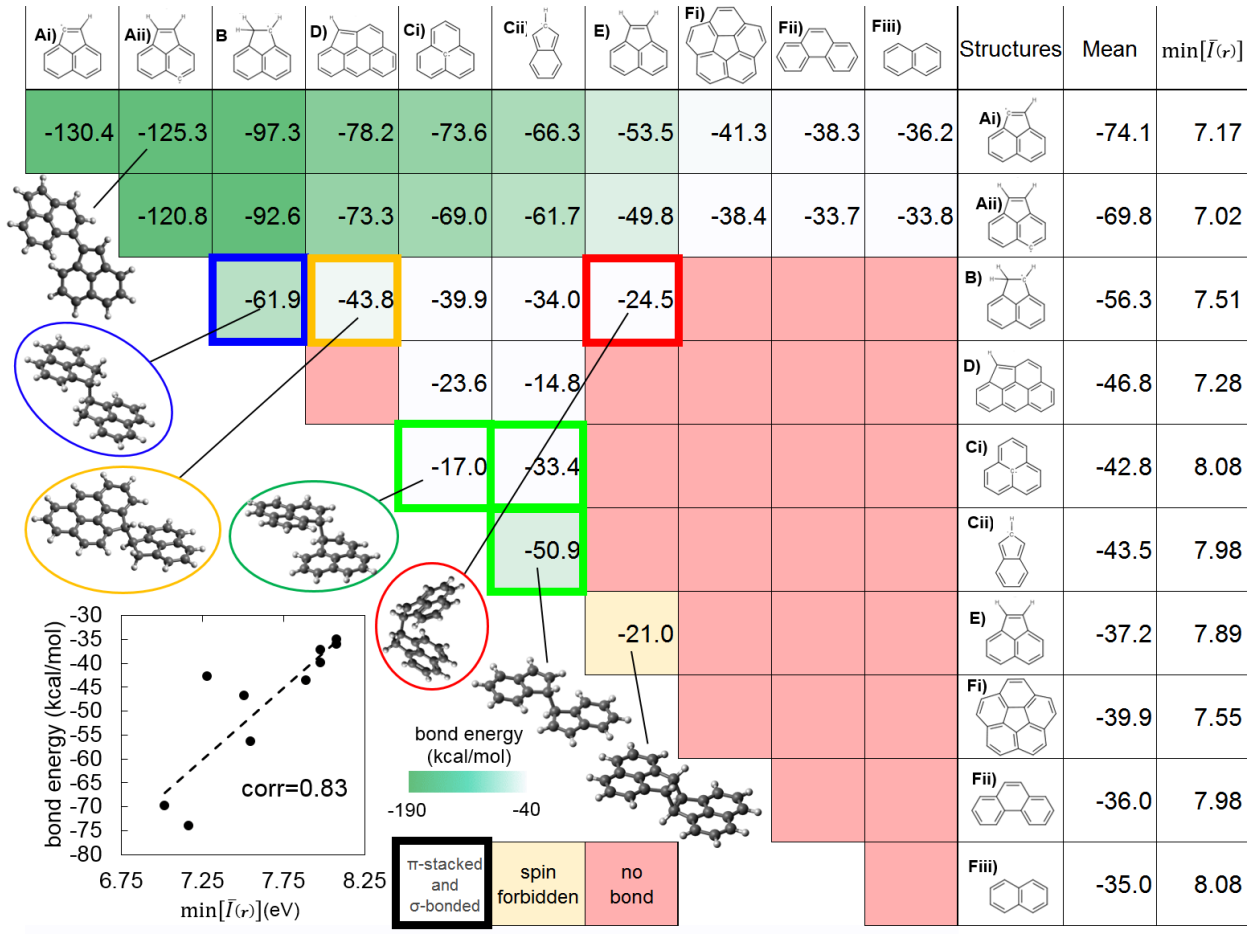

Figure 3: The bond energies (kcal/mol) between different species representing edge types shown in Figure 1. Inset graph shows the correlation between the bond energies and the $\bar{I}_S$ and a selection of geometries.

The most significant bond energies are formed with σ-radicals **(A)**, as shown by the first and second row of the grid in Figure 3. The bond energies follow the ordering suggested from $\bar{I}(\mathbf{r})$ for the radicals. The strongest bonds are formed with other sigma radicals with

< -120 kcal/mol. These bond energies are lower than single bond energies (-90 kcal/mol), indicating that these species are significantly conjugated and stabilised by delocalisation. We have previously demonstrated that crosslinking between two aromatics leads to a small drop in the band gap supporting such a limited conjugation.[59] The bond energy between two pentagonal ring σ-radicals **(Ai)** is particularly interesting as the minimum energy isomer is planar providing the greatest degree of delocalisation and the highest bond energy. This crosslink does not have steric hindence from the hydrogen and is therefore about to lie flat as has been observed in HR-AFM imaging.[12] This would provide for more effective van der Waals clustering . These σ-radical crosslinks would be long-lived in the flame based on the calculated bond energies. The next strongest crosslink with **(A)** is the localised π-radicals **(B)** with bond energies indicating single C–C bond formation between these edge types. Subsequent hydrogen abstraction could provide an **(Ai)** + **(Ai)** bond type, which as mentioned is favourable for clustering. The partially embedded pentagonal ring **(D)** also reacts readily with this site to form strong bonds (< -73 kcal/mol). The concentration of this site in flame aromatics is unknown and could be considerable given its possible equilibrium with hydrogen radicals and the methylated version as shown in Figure 2a.

Resonantly stabilised radicals crosslinking with σ-radicals **(A)**, suggested in the CHRCR mechanism,[13] follow with bond energies of < -61 kcal/mol. One question surrounding this crosslink is how the bond energy varies with the size of the RSR, as mentioned by Homann.[11] Computing the bond energies of site **(Aii)** with the small RSR indenyl **(Cii)** through to a 10-ring RSR species (shown in Figure 5) showed no decrease in the bond energy with system size with a mean value of -65.9 ± 2.8 kcal/mol. This indicates that while the bond energies with RSR are lower than a single bond, they do not vary greatly and that upon reaction with a σ-radical, the π-radical is easily localised to form a bond. This is somewhat anticipated from the size in-dependency of PAH growth processes on planar PAH,[22] which allows KMC schemes to grow large species given only local information of the PAH edge.[15,20,60?,61] Calculations have also shown that hydrogen can be easily lost from the RSR, reforming the radical and leading

to potential chain reactions.[13] However, the concentration of RSR in the flame needs to be determined to see how common these reactions could be. The presence of odd-numbered carbon species is not sufficient to established a RSR due to the hydrogenation of the edge, as has been recently demonstrated in HR-AFM; i.e., species with an odd number of carbon atoms that are protonated can become closed shell species.[21]

The reaction between a rim-based pentagonal ring **(E)** and a σ-radical **(A)** is the first step detailed in the AALH mechanism[19,20] and provides bond energies ~ -50 kcal/mol. For curved aromatics with low-aromaticity free edges **(Fi)** we found that bonds formed with **(A)** species were at the threshold of stability at flame temperatures, while crosslinks with phenanthrene **(Fii)** and naphthalene **(Fiii)** did not provide stable bonds at flame temperatures. The mechanisms including σ-radicals often require crosslinking followed by a hydrogen abstraction or loss to transform a weakened bonded structure into a **(A)** + **(A)** type crosslink. These mechanisms require a large number of σ-radicals and hydrogen radicals to allow for chemical polymerisations.[4] However, the high concentration of rim-based pentagons as has been seen in HR-AFM[21] makes these reactions of interest. In summary, crosslinking of σ-radicals providing strong bonds with energies < -40 kcal/mol with edge types **(Fi)**, **(E)**, **(C)**, **(D)** and **(B)**.

After the σ-radicals, the π-radicals are found to also form strong bonds with themselves and some high reactivity closed shell species. Localised π-radicals on rim-based pentagons **(B)**, row three of the table in Figure 3, forming bonds with itself of energy -62 kcal/mol. Bonds with **(D)** type edges are found to provide bonds below -40 kcal/mol while bonds with **(C)** and **(E)** type edges are above this threshold. Of particular interest are the bonds formed with the rim-based pentagonal rings **(E)** as these closed shell species are prevalent in the flame. The RSR radicals are found to form weak bonds with themselves and with the partially embedded pentagonal rings and no stable bonds with the rim-based pentagonal rings **(E)** were found to be possible. The exception is the small indenyl species that forms a strong bond with itself, **(Cii)** + **(Cii)**, showing that reactivity between RSR decreases with

the size of the species as indicated from the $\bar{I}_S$ for the less reactive π-radical (it should be recalled that this size dependency was not seen with the σ-radicals).

Finally, rim-based pentagonal rings **(E)** were found to form a weak bond with themselves, which is unlikely to be of interest. This [2+2] pericyclic reaction is not thermally allowed and requires optical excitation to form due to spin restrictions.[62] We have recently measured and calculated the band gap to be between 3.6–3.7 eV (≈350 nm deep UV).[59] These high energy photons are not prevalent in flames, indicating this bond is unlikely to form in a flame. The bond energy is also very low. Santos *et al.* have previously experimentally and computationally shown that the energetics of acenaphthylene dimerisation are not possible above 550 K,[62] further supporting the weak nature of these bonds.

From this systematic study, only σ-radicals **(A)** and localised π-radicals **(B)** are found to be capable of forming strong enough bonds to be long-lived in the flame. However, the π-radicals being able to bond on the aromatic face hold the possibility of combined physically held and covalently bound configurations, which is explored next.

Combining π-stacking and covalent bonding

As mentioned, physical dispersion forces are insufficient to stably bind clusters of small aromatic species at flame temperatures[4,35] and so covalently stabilised π-stacked structures are sought. The σ-radicals are unable to accomplish this feat as the reactive radical site points out from the aromatic ring, making bonding only achievable parallel to the aromatic planes, which will not allow for π-stacking. The thick-bordered entries in the matrix of Figure 3 show the reactive edges that were able to covalently bond as well as π-stack. These binding energies will be compared with van der Waals interactions and the unstrained covalent bonds, i.e. the energies of the covalent bond when there is no stacking from Figure 3.

Figure 4 shows the binding energy and molecular geometries of the reactive dimerisations for their average monomer mass. For comparison, physical dimerisation due to dispersion or van der Waals interactions have also been computed (black dashed lines). We have also

shown our benchmark SAPT(DFT) calculation from previous works, which can accurately predict the virial coefficient of benzene and the exfoliation energy of graphite (solid black lines).[42] From this we can see an overbinding of nonbonded planar aromatics by the hybrid density functional method M06-2X-D3, which we have previously seen for these empirically corrected DFT methods.[45] Given that this overbinding is linear in molecular mass, we can compare the enhancement $\Delta E = E_{VdW} - E_{C+VdW}$ due to any covalent interactions E_{C+VdW} compared to the van der Waals dimers E_{VdW} calculated with the dispersion corrected DFT for an equivalent mass monomer (blue and green arrows in Figure 4).

Figure 4a insets show the geometries of the single bonds formed between the species and, in the case of the localised π-bonds **(B)** as referred to in Figure 1, how rotation about the single bond does not impact the binding energy of these species. Figure 4b shows how as the molecular mass increases this binding is enhanced by van der Waals interactions, either by maintaining a rim-based bond across the fragments, in the case of **(B)** type edges, or through multicentre π-bonds, in the case of RSR **(C)** .

The localised π-radicals **(B)** are found to most strongly bind with themselves **(B)** having an average enhancement of some $\Delta E = 50 \pm 4$ kcal/mol. This is allowed for by the minimal strain in going from the unstacked species to the π-stacked configuration due to the ability of the saturated pentagonal ring hydrogens to be placed far from each other. These edges also form strong bonds with partially embedded pentagonal rings **(D)** with an enhancement of $\Delta E = 35 \pm 6$ kcal/mol. For the reaction of **(B)** with the rim-based pentagonal ring **(E)** we found a minor enhancement of $\Delta E = 8 \pm 4$ kcal/mol. This small enhancement might be explained by the low initial bond energy in the unstacked configuration. When stacked the added strain provides reduced bond energies.

Resonantly stabilised π-radicals are able to form multicentre π-bonds – a so-called "pancake bond" – and have been suggested to stabilise clustering aromatics.[38,64] We found enhancements of $\Delta E = 6 \pm 3$ kcal/mol compared with non-bonded configurations indicating a minor increase in binding energy. This is comparable to binding energies previously com-

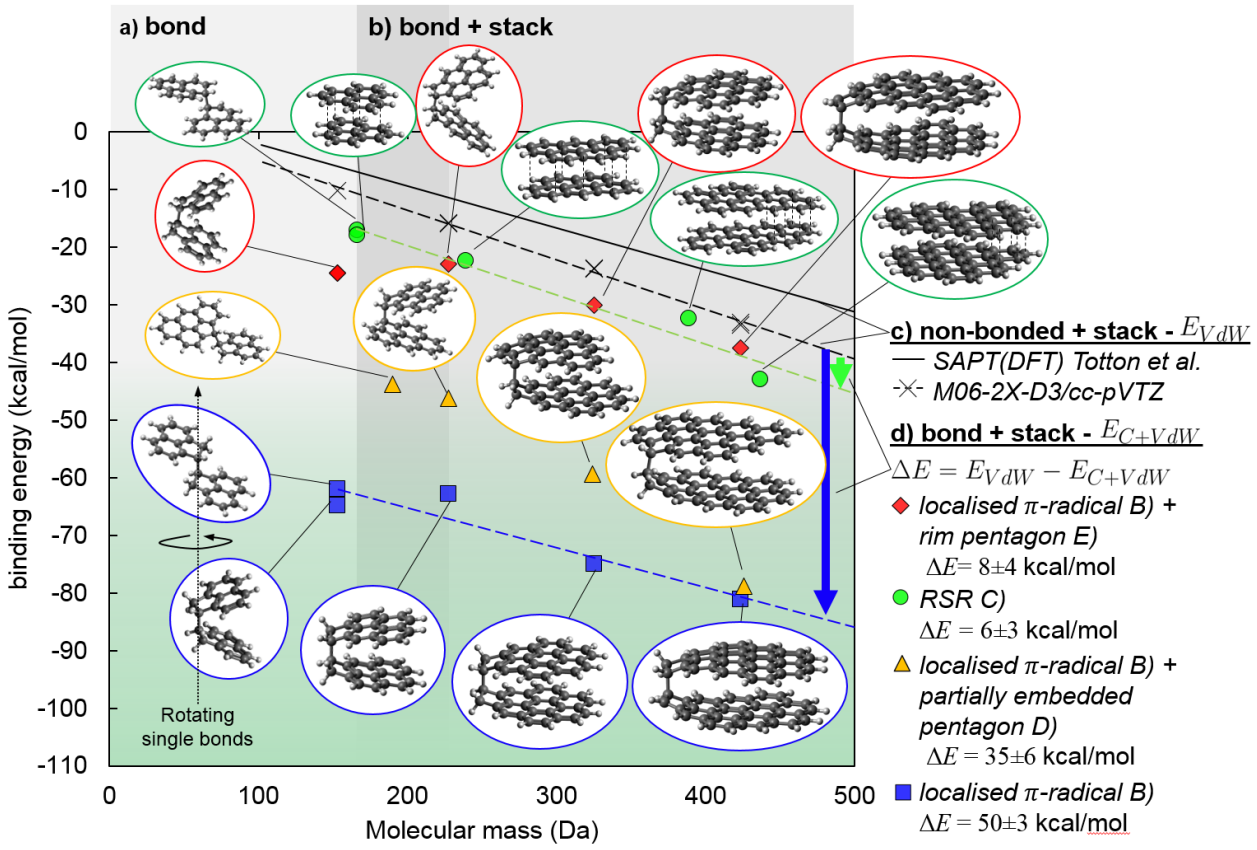

Figure 4: **a)** Binding energy (kcal/mol) as a function of molecular mass of the monomers (Da) is shown for different covalently bonded structures from Figure 3. **b)** Bonded and stacked geometries are found for enlarged monomers. **c)** Binding energy solely from van der Waals interactions E_{VdW} is also shown for comparison with the method chosen compared with our reference calculations from Totton et al.[63] **d)** The bonding enhancement compared with the non-bonded case ΔE is also shown.

puted.[54] We found that for the most stable isomers the multicentre bond was not formed across the entire molecule but was partially localised to the most triangulene-like part of the fragment. This is illustrated in Figure 5 where we have plotted the dimer orientation, monomer spin population and dimer HOMO of four of the RSR molecules. From the pancake bonding molecular orbital we can see that the multicentre bond is concentrated on one end of the dimer. This is geometrically manifested in the optimised structures where the region of bonding possesses a lower interlayer distance of 3.38 Å compared with the opposing edge of 3.7 Å. This can be understood from examining the spin population in Figure 5, indicating that the π-radical is concentrated on the most triangulene-like region of the molecule from where it forms the multicentre bond.

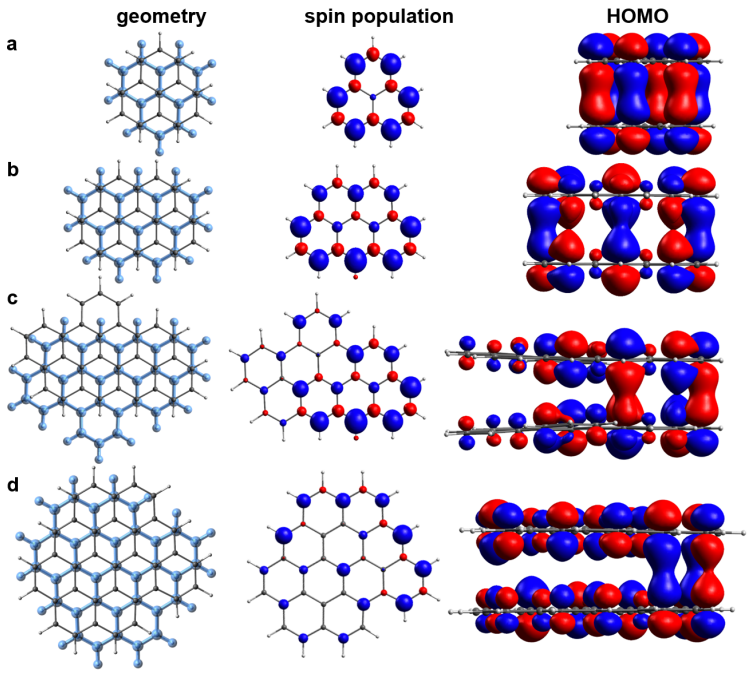

Figure 5: a-d) Dimer geometries, spin population at $iso = 0.003$ a.u. and HOMO at $iso = 0.025$ a.u. for a selection of RSRs showing the localisation of the radical on the most triangulene-like edge.

Considering the implications for soot formation. we can discuss whether these covalently bound complexes could allow for an explanation for the fluorescence signal interpreted as

stacked aromatic eximer state.[32] Recent calculations by Krueger and Blanquart of sp^3 bonded aromatics through aliphatics that are stacked showed that these long lived eximer states can indeed exist in stacked and bonded complexes.[65] Therefore, we anticipate that the localised π-radical **(B)** bonded complexes will possess a fluorescence signal. For the pancake bonded complexes, however, it is unclear whether an eximer state would be bound given that the $\pi \rightarrow \pi^*$ transition would be expected to lead to a breaking of the pancake bond. Pancake bonds are also highly phase dependent, breaking if they are rotated by 30°,[66] further questioning whether they could be stable at flame temperatures.

These novel stacked aromatic crosslinks, however, do provide some possible crosslinks for the covalently stabilised soot nucleation mechanism with high sticking coefficients that have been found to be computationally required for modelling soot nucleation.[6,36,37] In particular, the ability of multiple localised π-radicals to be formed on a single aromatic suggests that the rim-based pentagonal ring, in partial equilibrium with hydrogen radicals in the flame (as shown in Figure 2a), could provide a constant supply of reactive sites to polymerise soot formation.

Comparing these aromatically bonded complexes with aliphatically bridged species would also be of interest. This would require a full kinetic mechanism considering both the formation and fragmentation routes for both pathways. Both the aromatic and aliphatically bonded complexes have been shown to form bonds of sufficient energy to withstand flame temperatures,[55,65,67] however, both will be subject to radical induced fragmentation to varying degrees. Examples of this are hydrogen abstraction from aliphatics leading to β-scission that leads to the rapid fragmentation of aliphatic fuels[58] as well as hydrogen addition to polyynes leads also to radical induced fragmentation that inhibits growth of polyynes to <20 carbon atoms in size.[68,69] An example of this could be hydrogen addition to a **(Ai)**–**(Ai)** crosslink providing the **(Ai)**–**(E)** crosslink leading to a significant decrease in bond energy. Further hydrogen addition to the crosslink would give **(E)**–**(E)** that is not thermally stable at flame conditions. We anticipate aliphatic bridges will be particularly vulnerable to

hydrogen abstraction and thermal fragmentation through β-scissions.

Conclusions

The average local ionisation potential was used to locate and characterise the reactive edge sites that have been recently directly imaged in aromatic soot precursors. The radical sites and closed shell edge types were characterised with seven reactive edge types, which were detailed and compared. The location of reactive sites allowed for a systematic study of the bond energies between different covalently crosslinked reactive edge types. σ-radicals were found to form strong bonds with curved PAH low aromaticity free edges **(Fi)**, rim-based pentagonal ring free edges **(E)**, resonantly stabilised π-radicals **(C)**, partially embedded pentagonal ring edges **(D)** and localised π-radical on a partially saturated rim based pentagonal ring **(B)**, indicating the importance of such crosslinks in certain flame types. π-radicals possess lower covalent bond energies, however, they were found to allow for stacked and bonded configurations significantly enhancing the interaction energy as the monomers mass increased. Localised π-radicals **(B)** are suggested to be important due to their significant binding energy and the potential to rapidly generate them via protonation of abundant rim-based pentagonal rings. More work is required to determine the thermal stability of these covalently stabilised stacked complexes to radical induced fragmentation and to establish the concentration of each edge type within sooting flames. However, we have demonstrated that covalent bonds and stacked configurations are not necessarily mutually exclusive and that strongly bound complexes of interest to soot formation can be formed between aromatic soot precursors containing localised π-radicals on rim-based pentagonal rings.

ACKNOWLEDGEMENT

This project is supported by the National Research Foundation (NRF), Prime Minister's Office, Singapore under its Campus for Research Excellence and Technological Enterprise

(CREATE) programme.The project is also supported by National Science Foundation of China (91541122) and the Foundation of State Key Laboratory of Coal Combustion (FSKL-CCA1701). MK gratefully acknowledges the support of the Alexander von Humboldt foundation. We would like to thank Prof. Hai Wang and Prof. Andrea D'Anna for fruitful discussions.

SUPPORTING INFORMATION DESCRIPTION

Further calculations can be found in the supplementary information.

REFERENCES

(1) Landrigan, P. J.; Fuller, R.; Acosta, N. J. R.; Adeyi, O.; Arnold, R.; Basu, N. N.; Baldé, A. B.; Bertollini, R.; Bose-O'Reilly, S.; Boufford, J. I. et al. The Lancet Commission on pollution and health. *Lancet* **2017**,

(2) McConnell, J. R.; Edwards, R.; Kok, G. L.; Flanner, M. G.; Zender, C. S.; Saltzman, E. S.; Banta, J. R.; Pasteris, D. R.; Carter, M. M.; Kahl, J. D. W. 20th-Century industrial black carbon emissions altered arctic climate forcing. *Science* **2007**, *317*, 1381–1384.

(3) Bond, T. C.; Doherty, S. J.; Fahey, D. W.; Forster, P. M.; Berntsen, T.; Deangelo, B. J.; Flanner, M. G.; Ghan, S.; Kärcher, B.; Koch, D. et al. Bounding the role of black carbon in the climate system: A scientific assessment. *J. Geophys. Res.* **2013**, *118*, 5380–5552.

(4) Wang, H. Formation of nascent soot and other condensed-phase materials in flames. *Proc. Combust. Inst.* **2011**, *33*, 41 – 67.

(5) Rummel, K.; Veh, P.-O. Die Strahlung Leuchtender Flammen. Erster Teil: Schrifttumsgrundlagen, Arbeitshypothesen und Vorversuche (Translation: The radiance of glowing

flames. Part 1: Foundations, working hypotheses and preliminary experiments). *Archiv für das Eisenhüttenwesen* **1941**, *14*, 489–499.

(6) Harris, S. J.; Weiner, A. M. A picture of soot particle inception. *Symp. (Int.) Combust., [Proc.]* **1989**, *22*, 333 – 342.

(7) Hou, D.; You, X. Reaction kinetics of hydrogen abstraction from polycyclic aromatic hydrocarbons by H atoms. *Phys. Chem. Chem. Phys.* **2017**, *19*, 30772–30780.

(8) Frenklach, M.; Clary, D. W.; Gardiner Jr, W. C.; Stein, S. E. Detained kinetic modeling of soot formation in shock-tube pyrolysis of acetylene. *Symp. (Int.) Combust., [Proc.]* **1985**, *20*, 887–901, Twentieth Symp. (Int.) Combust., [Proc.].

(9) Frenklach, M. Reaction mechanism of soot formation in flames. *Phys. Chem. Chem. Phys.* **2002**, *4*, 2028–2037.

(10) Hansen, N.; Cool, T. A.; Westmoreland, P. R.; Kohse-Höinghaus, K. Recent contributions of flame-sampling molecular-beam mass spectrometry to a fundamental understanding of combustion chemistry. *Prog. Energy Combust. Sci.* **2009**, *35*, 168–191.

(11) Keller, A.; Kovacs, R.; Homann, K.-H. Large molecules, ions, radicals and small soot particles in fuel-rich hydrocarbon flames. Part IV. Large polycyclic aromatic hydrocarbons and their radicals in a fuel-rich benzene–oxygen flame. *Phys. Chem. Chem. Phys.* **2000**, *2*, 1667–1675.

(12) Schulz, F.; Commodo, M.; Kaiser, K.; Falco, G. D.; Minutolo, P.; Meyer, G.; D'Anna, A.; Gross, L. Insights into incipient soot formation by atomic force microscopy. *Proc. Combust. Inst.* **2019**, *37*, 885 – 892.

(13) Johansson, K.; Head-Gordon, M.; Schrader, P.; Wilson, K.; Michelsen, H. Resonance-stabilized hydrocarbon-radical chain reactions may explain soot inception and growth. *Science* **2018**, *361*, 997–1000.

(14) Frenklach, M.; Schuetz, C. A.; Ping, J. Migration mechanism of aromatic-edge growth. *Proc. Combust. Inst.* **2005**, *30*, 1389–1396.

(15) Whitesides, R.; Frenklach, M. Detailed kinetic Monte Carlo simulations of graphene-edge growth. *J. Phys. Chem. A* **2009**, *114*, 689–703.

(16) Clar, E.; McAndrew, B.; Zander, M. The establishment of double bond character in methyl derivatives of phenanthrene, pyrene, chrysene and coronene by NMR. *Tetrahedron* **1967**, *23*, 985–993.

(17) Stein, S. E.; Fahr, A. High-temperature stabilities of hydrocarbons. *J. Phys. Chem.* **1985**, *89*, 3714–3725.

(18) Howard, J. B. Carbon addition and oxidation reactions in heterogeneous combustion and soot formation. *Symp. (Int.) Combust., [Proc.]* **1991**, *23*, 1107–1127.

(19) D'Anna, A.; Violi, A.; D'Alessio, A.; Sarofim, A. F. A reaction pathway for nanoparticle formation in rich premixed flames. *Combust. Flame* **2001**, *127*, 1995–2003.

(20) Violi, A.; Kubota, A.; Truong, T.; Pitz, W.; Westbrook, C.; Sarofim, A. A fully integrated kinetic monte carlo/molecular dynamics approach for the simulation of soot precursor growth. *Proc. Combust. Inst.* **2002**, *29*, 2343–2349.

(21) Commodo, M.; Kaiser, K.; De Falco, G.; Minutolo, P.; Schulz, F.; D'Anna, A.; Gross, L. On the early stages of soot formation: Molecular structure elucidation by high-resolution atomic force microscopy. *Combust. Flame* **2019**, *205*, 154–164.

(22) Raj, A. Structural effects on the growth of large polycyclic aromatic hydrocarbons by C_2H_2. *Combust. Flame* **2019**, *204*, 331 – 340.

(23) Lafleur, A. L.; Howard, J. B.; Taghizadeh, K.; Plummer, E. F.; Scott, L. T.; Necula, A.; Swallow, K. C. Identification of $C_{20}H_{10}$ sicyclopentapyrenes in flames: Correlation with corannulene and fullerene formation. *J. Phys. Chem.* **1996**, *100*, 17421–17428.

(24) Martin, J. W.; Botero, M.; Slavchov, R. I.; Bowal, K.; Akroyd, J.; Mosbach, S.; Kraft, M. Flexoelectricity and the formation of carbon nanoparticles in flames. *J. Phys. Chem. C* **2018**, *122*, 22210–22215.

(25) Martin, J. W.; Slavchov, R. I.; Yapp, E. K. Y.; Akroyd, J.; Mosbach, S.; Kraft, M. The polarization of polycyclic aromatic hydrocarbons curved by pentagon incorporation: the role of the flexoelectric dipole. *J. Phys. Chem. C* **2017**, *121*, 27154–27163.

(26) Dobrowolski, M. A.; Ciesielski, A.; Cyrański, M. K. On the aromatic stabilization of corannulene and coronene. *Phys. Chem. Chem. Phys.* **2011**, *13*, 20557–20563.

(27) Su, D.; Jentoft, R.; Müller, J.-O.; Rothe, D.; Jacob, E.; Simpson, C.; Tomović, Z.; Müllen, K.; Messerer, A.; Pöschl, U. et al. Microstructure and oxidation behaviour of Euro IV diesel engine soot: a comparative study with synthetic model soot substances. *Catal. Today* **2004**, *90*, 127 –132, Air Pollution Abatement Symposium.

(28) Raj, A.; Yang, S. Y.; Cha, D.; Tayouo, R.; Chung, S. H. Structural effects on the oxidation of soot particles by O_2: Experimental and theoretical study. *Combust. Flame* **2013**, *160*, 1812 – 1826.

(29) Frenklach, M.; Liu, Z.; Singh, R. I.; Galimova, G. R.; Azyazov, V. N.; Mebel, A. M. Detailed, sterically-resolved modeling of soot oxidation: Role of O atoms, interplay with particle nanostructure, and emergence of inner particle burning. *Combust. Flame* **2018**, *188*, 284–306.

(30) Happold, J.; Grotheer, H.-H.; Aigner, M. In *Combustion Generated Fine Carbonaceous Particles*; Bockhorn, H., Ed.; KIT Scientific Publishing, Karlsruhe, Germany, 2009; Chapter 18, pp 277 – 288.

(31) Carbone, F.; Canagaratna, M. R.; Lambe, A. T.; Jayne, J. T.; Worsnop, D. R.; Gomez, A. Exploratory analysis of a sooting premixed flame via on-line high resolution (APi-TOF) mass spectrometry. *Proc. Combust. Inst.* **2018**, *37*, 1–8.

(32) Miller, J. H. Aromatic excimers: evidence for polynuclear aromatic hydrocarbon condensation in flames. *Proc. Combust. Inst.* **2005**, *30*, 1381–1388.

(33) Sirignano, M.; Collina, A.; Commodo, M.; Minutolo, P.; D'Anna, A. Detection of aromatic hydrocarbons and incipient particles in an opposed-flow flame of ethylene by spectral and time-resolved laser induced emission spectroscopy. *Combust. Flame* **2012**, *159*, 1663 – 1669.

(34) Mercier, X.; Carrivain, O.; Irimiea, C.; Faccinetto, A.; Therssen, E. Dimers of polycyclic aromatic hydrocarbons: the missing pieces in the soot formation process. *Phys. Chem. Chem. Phys.* **2019**, *21*, 8282–8294.

(35) Totton, T. S.; Misquitta, A. J.; Kraft, M. A quantitative study of the clustering of polycyclic aromatic hydrocarbons at high temperatures. *Phys. Chem. Chem. Phys.* **2012**, *14*, 4081–94.

(36) Miller, J. H. The kinetics of polynuclear aromatic hydrocarbon agglomeration in flames. *Symp. (Int.) Combust., [Proc.]* **1991**, *23*, 91 – 98, Twenty-Third Symp. (Int.) Combust., [Proc.].

(37) Kholghy, M. R.; Kelesidis, G. A.; Pratsinis, S. E. Reactive polycyclic aromatic hydrocarbon dimerization drives soot nucleation. *Phys. Chem. Chem. Phys.* **2018**, *20*, 10926–10938.

(38) Vitiello, G.; De Falco, G.; Picca, F.; Commodo, M.; D'Errico, G.; Minutolo, P.; D'Anna, A. Role of radicals in carbon clustering and soot inception: A combined EPR and Raman spectroscopic study. *Combust. Flame* **2019**, *205*, 286–294.

(39) Bulat, F. A.; Burgess, J. S.; Matis, B. R.; Baldwin, J. W.; Macaveiu, L.; Murray, J. S.; Politzer, P. Hydrogenation and fluorination of graphene models: Analysis via the average local ionization Energy. *J. Phys. Chem. A* **2012**, *116*, 8644–8652.

(40) Zhao, Y.; Truhlar, D. G. The M06 suite of density functionals for main group thermochemistry, thermochemical kinetics, noncovalent interactions, excited states, and transition elements: two new functionals and systematic testing of four M06-class functionals and 12 other functionals. *Theoretical Chemistry Accounts* **2008**, *120*, 215–241.

(41) Wang, Y.; Verma, P.; Jin, X.; Truhlar, D. G.; He, X. Revised M06 density functional for main-group and transition-metal chemistry. *Proceedings of the National Academy of Sciences* **2018**, *115*, 10257–10262.

(42) Totton, T. S.; Misquitta, A. J.; Kraft, M. Assessing the polycyclic aromatic hydrocarbon anisotropic potential with application to the exfoliation energy of graphite. *J. Phys. Chem. A* **2011**, *115*, 13684–13693.

(43) Frisch, M. J.; Trucks, G. W.; Schlegel, H. B.; Scuseria, G. E.; Robb, M. A.; Cheeseman, J. R.; Scalmani, G.; Barone, V.; Petersson, G. A.; Nakatsuji, H. et al. Gaussian 09, Revision A 02. 2009.

(44) Grimme, S. Semiempirical GGA-type density functional constructed with a long-range dispersion correction. *J. Comput. Chem.* **2006**, *27*, 1787–1799.

(45) Martin, J. W.; McIntosh, G. J.; Arul, R.; Oosterbeek, R. N.; Kraft, M.; Söhnel, T. Giant fullerene formation through thermal treatment of fullerene soot. *Carbon* **2017**, *125*, 132–138.

(46) Martin, J. W.; Bowal, K. L.; Menon, A.; Slavchov, R. I.; Akroyd, J.; Mosbach, S.; Kraft, M. Polar curved polycyclic aromatic hydrocarbons in soot formation. *Proc. Combust. Inst.* **2019**, *37*, 1117–1123.

(47) Sjoberg, P.; Murray, J. S.; Brinck, T.; Politzer, P. Average local ionization energies on the molecular surfaces of aromatic systems as guides to chemical reactivity. *Can. J. Chem.* **1990**, *68*, 1440–1443.

(48) Yuan, H.; Kong, W.; Liu, F.; Chen, D. Study on soot nucleation and growth from PAHs and some reactive species at flame temperatures by ReaxFF molecular dynamics. *Chem. Eng. Sci.* **2019**, *195*, 748 – 757.

(49) Toro-Labbé, A.; Jaque, P.; Murray, J. S.; Politzer, P. Connection between the average local ionization energy and the Fukui function. *Chem. Phys. Lett.* **2005**, *407*, 143 – 146.

(50) Lu, T.; Chen, F. Multiwfn: a multifunctional wavefunction analyzer. *J. Comput. Chem.* **2012**, *33*, 580–592.

(51) Balaban, A. T.; Klein, D. J. Claromatic carbon nanostructures. *J. Phys. Chem. C* **2009**, *113*, 19123–19133.

(52) Solà, M. Forty years of Clar's aromatic π-sextet rule. *Front. Chem.* **2013**, *1*, 22.

(53) Liu, M.; Green, W. H. Capturing aromaticity in automatic mechanism generation software. *Proc. Combust. Inst.* **2019**, *37*, 575 – 581.

(54) Kertesz, M. Pancake bonding: An unusual pi-stacking interaction. *Chem. - Eur. J.* **2019**, *25*, 400–416.

(55) Adamson, B. D.; Skeen, S. A.; Ahmed, M.; Hansen, N. Detection of aliphatically bridged multi-core polycyclic aromatic hydrocarbons in sooting flames with atmospheric-sampling High-Resolution Tandem Mass Spectrometry. *J. Phys. Chem. A* **2018**, *122*, 9338–9349.

(56) Neutral Thermochemical Data. In NIST Chemistry WebBook, volume = Standard Reference Database Number 69 author = Afeefy, H.Y. and Liebman, J. F and Stein, S. E., publisher = National Institute of Standards and Technology, address = Gaithersburg, MD, howpublished = `http://webbook.nist.gov`, note = retrieved: June 20, 2019, doi = 10.18434/T4D303.

(57) Tranter, R. S.; Klippenstein, S. J.; Harding, L. B.; Giri, B. R.; Yang, X.; Kiefer, J. H. Experimental and theoretical investigation of the self-reaction of phenyl radicals. *J. Phys. Chem. A* **2010**, *114*, 8240–8261.

(58) Ratkiewicz, A.; Truong, T. N. Kinetics of the CC Bond Beta Scission Reactions in Alkyl Radical Reaction Class. *J. Phys. Chem. A* **2012**, *116*, 6643–6654.

(59) Menon, A.; Dreyer, J.; Martin, J. W.; Akroyd, J.; Robertson, J.; Kraft, M. Optical band gap of cross-linked, curved, and radical polyaromatic hydrocarbons. *Phys. Chem. Chem. Phys.* **2019**,

(60) Frenklach, M. On surface growth mechanism of soot particles. *Symposium (International) on Combustion* **1996**, *26*, 2285–2293.

(61) Raj, A.; Celnik, M.; Shirley, R.; Sander, M.; Patterson, R.; West, R.; Kraft, M. A statistical approach to develop a detailed soot growth model using PAH characteristics. *Combustion and Flame* **2009**, *156*, 896 – 913.

(62) Santos, R. C.; Bernardes, C. E.; Diogo, H. P.; Piedade, M. F. M.; Canongia Lopes, J. N.; Minas da Piedade, M. E. Energetics of the thermal dimerization of acenaphthylene to heptacyclene. *J. Phys. Chem. A* **2006**, *110*, 2299–2307.

(63) Totton, T. S.; Misquitta, A. J.; Kraft, M. A quantitative study of the clustering of polycyclic aromatic hydrocarbons at high temperatures. *Phys. Chem. Chem. Phys.* **2012**, *14*, 4081–4094.

(64) Small, D.; Rosokha, S. V.; Kochi, J. K.; Head-Gordon, M. Characterizing the dimerizations of phenalenyl radicals by ab initio calculations and spectroscopy: σ-Bond formation versus resonance π-stabilization. *J. Phys. Chem. A* **2005**, *109*, 11261–11267.

(65) Krueger, R. A.; Blanquart, G. Predicting aromatic exciplex fluorescence emission energies. *Phys. Chem. Chem. Phys.* **2019**, 10325–10335.

(66) Cui, Z.-H.; Lischka, H.; Beneberu, H. Z.; Kertesz, M. Rotational barrier in phenalenyl neutral radical dimer: Separating pancake and van der Waals interactions. *J. Am. Chem. Soc.* **2014**, *136*, 5539–5542.

(67) Giordana, A.; Maranzana, A.; Tonachini, G. Carbonaceous nanoparticle molecular inception from radical addition and van der Waals coagulation of polycyclic aromatic hydrocarbon-based systems. A theoretical study. *J. Phys. Chem. C* **2011**, *115*, 17237–17251.

(68) Gerhardt, P.; Homann, K. d. Ions and charged soot particles in hydrocarbon flames. 2. Positive aliphatic and aromatic ions in ethyne/oxygen flames. *J. Phys. Chem.* **1990**, *94*, 5381–5391.

(69) Maricq, M. M. An examination of soot composition in premixed hydrocarbon flames via laser ablation particle mass spectrometry. *J. Aerosol Sci.* **2009**, *40*, 844 – 857.

TOC IMAGE

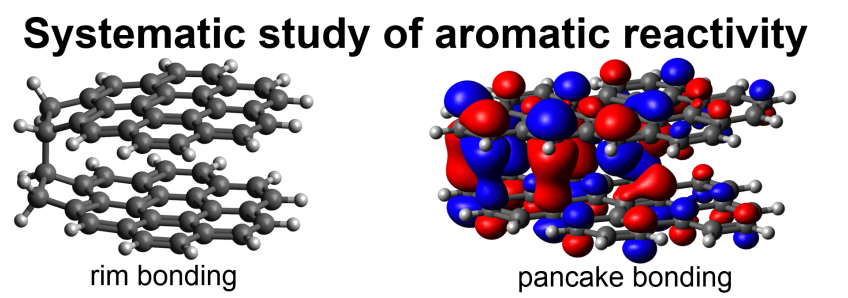
Systematic study of aromatic reactivity
rim bonding
pancake bonding
π-radicals combine bonding and stacking